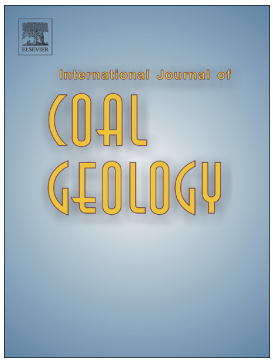

Fast and accurate shale maturity determination by Raman spectroscopy measurement with minimal sample preparation

Bastian Sauerer, Paul R. Craddock, Mohammed D. AlJohani, Khalid L. Alsamadony, Wael Abdallah

PII: S0166-5162(16)30768-6
DOI: doi: 10.1016/j.coal.2017.02.008
Reference: COGEL 2791

To appear in: *International Journal of Coal Geology*

Received date: 24 November 2016
Revised date: 16 February 2017
Accepted date: 16 February 2017

Please cite this article as: Bastian Sauerer, Paul R. Craddock, Mohammed D. AlJohani, Khalid L. Alsamadony, Wael Abdallah , Fast and accurate shale maturity determination by Raman spectroscopy measurement with minimal sample preparation. The address for the corresponding author was captured as affiliation for all authors. Please check if appropriate. Cogel(2017), doi: 10.1016/j.coal.2017.02.008

Fast and Accurate Shale Maturity Determination by Raman Spectroscopy Measurement with Minimal Sample Preparation

Bastian Sauerer[a,*], Paul R. Craddock[b], Mohammed D. AlJohani[a], Khalid L. Alsamadony[a], Wael Abdallah[a]

[a] Schlumberger Middle East, S.A., Schlumberger Dhahran Carbonate Research Center, Dhahran Techno Valley, P.O. Box 39011, Dammam 31942, Saudi Arabia.
[b] Schlumberger Doll Research Center, One Hampshire St., Cambridge, MA 02139, USA.

* Corresponding Author.
Email address: bsauerer@slb.com (B. Sauerer).

Abstract

This study presents a robust correlation between Raman spectroscopy signal (expressed as the Raman band separation) and thermal maturity obtained by the vitrinite reflectance technique. The organic-rich mudstones used to build this correlation originate from a variety of paleo-marine sedimentary basins. The resulting correlation enables thermal maturity of kerogen expressed as vitrinite reflectance equivalent to be estimated in unknown formation samples using Raman spectroscopy. Raman spectroscopy can thus be used for determination of maturation windows (immature, oil, wet gas, or dry gas). Moreover, different to other Raman measurements that are performed on isolated kerogen or on polished surfaces of drill core and cutting fragments, the technique here is executed directly on fragments with minimal preparation, making it potentially applicable for wellsite maturity estimations. It is further shown that differences in the Raman analysis of kerogen seen among different published studies can be ascribed in part to the use of different Raman laser wavelengths. Taking wavelength dependence into account, the maturity determination of organic-rich mudstones by Raman spectroscopy may be developed into a generalized method, independent of the instrumental setup.

Keywords: Shale, Maturity, Raman Spectroscopy, Kerogen

1. Introduction

Depletion of conventional carbonate and sandstone reservoirs has led to recent exploration and production of so-called unconventional petroleum resources, in particular of petroleum source rocks, organic-rich mudstones commonly referred to as shales (Blyth et al., 1984). So far, the United States, Canada, and China are the only countries producing natural gas in commercial volumes from organic-rich mudstones (Aloulou, 2015). Development of these resources requires state-of-the-art and integrated drilling and completion techniques, posing significant financial burden on operators and rendering much of this resource unprofitable in times of low commodity prices. Technological advances in the characterization of organic-rich mudstones will play a key role in producing more cost effectively from these formations.

Organic-rich mudstones are composed of fine-grained minerals that form rock layers with extremely low (micro- to nano-Darcy) permeability. Organic matter, predominantly kerogen formed from the burial and preservation of fossil living matter, is interspersed within the mineral matrix (Hutton et al., 1994). Under heat and pressure, kerogen thermally decomposes into petroleum (bitumen, oil, and gas), and non-petroleum products such as CO_2, N_2, and H_2S (Peters et al., 2004). The thermal maturation of kerogen is also referred to as graphitization. This process can be grossly described by the loss of heteroatoms (N, S, and O) and hydrogen-rich (aliphatic carbon) groups, leaving a kerogen residue that is hydrogen-poor and dominated by aromatic carbon structures. The extreme endmember of kerogen decomposition, under metamorphic conditions, is the formation of pure carbon in the form of graphite (Rantitsch et al., 2016; Hood et al., 1975). The amount of petroleum generated is a function of kerogen type and initial content in the formation, and the magnitude and duration in which heat and pressure were applied (McCarthy et al., 2011).

Conventionally, thermal maturity of kerogen is determined by optical inspection of vitrinite macerals, known as vitrinite reflectance (Diessel et al., 1978). This technique requires significant expertise and is labor intensive (Hackley et al., 2015). A common challenge for this method is the correct distinction of vitrinite from other macerals such as solid bitumen, semi-fusinite, and inertinite (Hackley et al., 2015). More significantly, this technique is impractical in formations that lack vitrinite. This is especially problematic in sedimentary formations older than the Devonian, prior to the evolution of vitrinite-rich land plants. There have been efforts to measure the reflectance of graptolites or chitinozoans that, similar to vitrinite, express a change in reflectance during maturation (Cardott and Kidwai, 1991; Petersen et al., 2013). Although it is possible to convert the measured reflectance of these zooclasts to vitrinite reflectance equivalent values, these correlations are not always straight forward due to reflectance anisotropy (Cole, 1994; Goodarzi, 1985a, 1985b; Petersen et al., 2013; Rantitsch, 1995). A second common method for estimating thermal maturity is Rock-Eval pyrolysis in which a formation sample is subject to programmed heating (Behar et al., 2001; Lafargue et al., 1998; Peters, 1986). The temperature at which the maximum amount of hydrocarbons is generated from decomposition of kerogen (the *S2* peak) is called T_{max}, which has been calibrated to vitrinite reflectance (Jarvie et al., 2001). Experience has shown that this approach commonly fails in organic-lean formations and/or formations that are thermally mature because the resulting *S2* peak is small (*S2* ≤ 1 mg HC/g rock) and the T_{max} estimate is unreliable. X-ray diffraction (Grew, 1974; Landis, 1971; Nishimura et al., 2000) and high-resolution transmission electron microscopy (Beyssac et al. 2002a; Bonijoly et al., 1982; Buseck and Huang, 1985) methods have also been used to examine graphitization of organic matter, but these approaches are generally limited

to metamorphic conditions at which organic materials develop well-defined crystal lattice structures, significantly above the range of temperature and pressure conditions relevant to the maturation of kerogen in source rocks. Moreover, the methods for XRD sample preparation involving grinding of the material generally render this approach as destructive (e.g., Wopenka and Pasteris, 1993).

Raman spectroscopy offers potential for rapid and non-destructive measurements for maturity estimates of petroleum source rocks. Raman spectroscopy has been widely used to characterize the structure of carbonaceous materials (Ferralis et al., 2016; Kelemen and Fang, 2001; Liu et al., 2013; Liu et al., 2016; Marshall et al., 2010; Pasteris and Wopenka, 1991; Schmidt Mumm and İnan, 2016; Spötl et al., 1998; Tuinstra and Koenig, 1970; Yui et al., 1996). Raman scattering is a function of the molecular vibrations and symmetries of chemical bonds. Raman spectroscopy offers a high spatial resolution in the micrometer range (Marshall et al., 2012). The fundamental physics of Raman scattering on graphitic material have been described in earlier publications (Tuinstra and Koenig, 1970). The first-order Raman spectrum of kerogen consists of two main peaks (Cesare and Maineri, 1999; Marshall et al., 2010). The G band appears at ~1600 cm^{-1} and is indicative of well-ordered, graphite-like carbon structures in the kerogen. The origin of the G band is due to the in-plane E_{2g2} vibrational modes of the carbon atoms in aromatic ring structures (sp^2 carbon) exhibiting D^4_{6h} symmetry. The D band appears at ~1350 cm^{-1} and results from Raman-active A_{1g} symmetry associated with lattice defects and discontinuities of the sp^2 carbon network. These defects were found to be attributed to in-plane heteroatoms and tetrahedral carbons that are released in the early part of the maturation process (Beyssac et al., 2002b). It has been observed that the G and D peaks shift towards higher and lower wavelengths, respectively, as maturity of the kerogen increases. The Raman band separation (RBS), which is the wavelength separation between the G and D peaks, has been proposed as a reliable maturity indicator (Kelemen and Fang, 2001).

In this study, we develop a robust correlation between RBS and vitrinite reflectance (%Ro). The maturity correlation is built using a set of organic-rich mudstone samples from multiple paleo-marine sedimentary basins containing predominantly Type II kerogen that span a range of ages and a wide range of vitrinite reflectance from 0.6 to >4 %Ro. The use of a short laser wavelength and successful fluorescence suppression allows the acquisition of high quality Raman spectra, even for immature mudstone samples that typically show intense fluorescence (Lünsdorf, 2016; Schmidt Mumm and İnan, 2016). The correlation provides a reference from which to accurately estimate thermal maturity of organic-rich mudstones using Raman spectroscopy measurements.

2. Materials and Methods

2.1. Samples

The eleven samples chosen for this study come from multiple organic-rich mudstone formations, predominantly from paleo-marine deposits of North America (Table 1). The age of the samples ranges from ~ 380 to 80 Ma and their total organic carbon (TOC) content ranges between 4 and 16 wt%. Sedimentary organic matter (kerogen) in the samples is predominantly marine Type II. Thermal maturity reference values (0.6 to 4.3 %Ro) were provided by external laboratories prior to the study, using conventional vitrinite reflectance optical inspection.

Samples were obtained as 5–10 gram splits from either drill core (side-wall plugs) or cuttings. Cores were roughly chipped to pieces approximately 10–20 mm in diameter. Cuttings pieces were typically 10 mm or less in diameter and did not undergo further size reduction. Core and cutting samples were cleaned using dichloromethane to remove native, soluble hydrocarbons and any residual drilling fluid. Approximately 1 gram splits of each sample were crushed to fine powder and sent to an external laboratory for total organic carbon (TOC) and Rock-Eval pyrolysis. Here, TOC concentrations reflect the carbon contribution only from kerogen and the data were used to confirm the presence of disseminated organic matter prior to Raman analysis. The Rock-Eval T_{max} values from the *S2* peak were used to estimate thermal maturity as further validation of the reference vitrinite reflectance values. The two techniques show good agreement up to thermal maturity ~ 1.4 %Ro, above which the Rock-Eval *S2* peak is too low (< 1 mg HC/g rock) to obtain a reliable T_{max} estimate.

2.2. Raman measurements

Raman spectroscopic measurements were made on sample chips without further preparation. The samples were not polished as this was observed to yield alteration of the Raman signal, most likely due to the creation of additional defects by mechanical abrasion, which could result in biased maturity estimates. Raman spectra were acquired using a Thermo Scientific DXR™ Raman Microscope. Monochromatic excitation was performed with a 532 nm laser, which was focused on the sample with a 10× magnification objective resulting in an estimated spot size of 2.1 μm. Laser wavelength calibration, white light calibration, and laser frequency calibration were performed before measuring the samples. Laser power was set to 10 mW. A 25 μm slit was used as aperture. The grating was set to 1800 lines/mm. Spectra were acquired from 1877 to 200 cm^{-1}. The Raman spectra were acquired and processed using OMNIC v9.3.03 software. Automated fluorescence correction was applied. For each sample, 25 spectra were collected at different locations on the sample surface, representing different topological features. Each spectrum is an average of 16 scans. Acquisition of each spectrum is less than 2 minutes. The so-called G and D bands are the two Raman spectral features most commonly studied in carbonaceous materials (Beyssac et al., 2002a, 2002b, 2003; Cesare and Maineri, 1999; Ferralis et al., 2016; Ferrari, 2002; Tuinstra and Koenig, 1970; Kelemen and Fang, 2001; Liu et al., 2013; Liu et al., 2016; Lünsdorf, 2016; Lünsdorf et al., 2014; Marshall et al., 2012; Matthews et al., 1999; Pasteris and Wopenka, 1991; Pócsik et al., 1998; Rantitsch et al., 2004; Schmidt Mumm and İnan, 2016; Spötl et al., 1998; Vidano et al., 1981; Wang et al., 1990; Yui et al., 1996). Following procedures established by earlier studies (Beyssac et al., 2003; Lünsdorf et al., 2014), deconvolution and fitting of the Raman spectra were made using five peaks with mixed Gaussian/Lorentzian profiles and a linear baseline correction (Fig. 1). No constraints were put on the peak parameters in the curve fitting procedure to allow an optimal fit to the measured spectra. The band positions, amplitudes (intensities), full-widths at half maximum, and integrated areas of all peaks were extracted from the resulting curve fits. It was found that, although the 25 spectra for each sample showed significant ranges in the peak widths, intensities, and areas, the mean G and D1 band positions and the mean RBS could be reliably extracted from the spectra with an average deviation of ± 2.7 cm^{-1}.

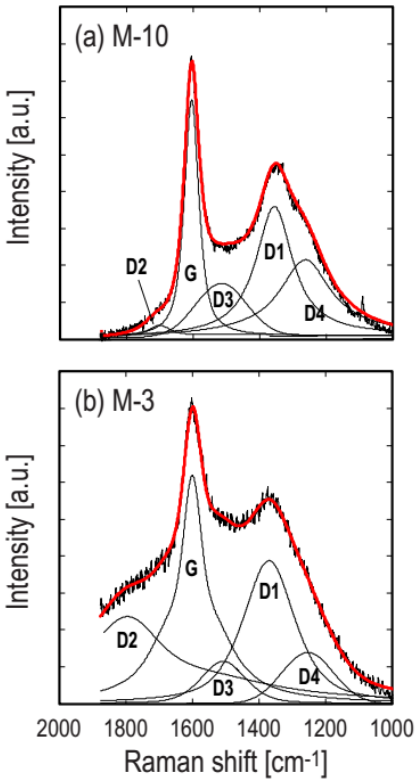

Fig. 1. Exemplary spectral deconvolution and Raman band identification: (a) sample M-10 and (b) sample M-3. The measured spectra are shown in black. The reconstructed spectra from the curve fitting using a graphitic band (G) and four defect bands (D1-D4) for each spectrum are shown by the red lines. G and D1 peak positions were reliably extracted from the curve fitting.

3. Results and Discussion

3.1. Raman maturity indices

Fig. 2 shows measured Raman kerogen spectra for all mudstones studied here, stacked in order of their vitrinite reflectance. All but one sample gave clean Raman spectra with clearly identifiable, characteristic G and D bands as is typical for kerogen. The exception is sample M-1, for which the spectra has low signal-to-noise and poorly resolvable bands. Sample M-1 contains predominantly Type IIS kerogen (sulfur-rich, > 13 wt% S), and the unique composition of this sample appears to detrimentally impact the Raman measurement. Previous Raman studies have documented systematic changes in both the positions and areas of the D1 and G bands in the Raman spectra of carbonaceous materials as a function of thermal maturity (Beyssac et al., 2002a, 2002b; Kelemen and Fang, 2001; Liu et al., 2013; Pasteris and Wopenka, 1991; Schmidt Mumm and İnan, 2016; Spötl et al., 1998; Yui et al., 1996): The G and D1 band positions (W_G and W_{D1}) separate, and the G and D1 band areas (A_G and A_{D1}) increase and decrease, respectively, during thermal maturation. Fig. 2 shows qualitatively that the band positions for the samples examined here widen with increasing thermal maturity, consistent with results from earlier studies. Two common types of Raman thermal maturity indicators have been extracted from Raman spectra: (1) Raman band separation, RBS = W_G – W_{D1} from G and D1 band positions (Table 1, Fig. 3) and (2) Raman band ratios based on band intensities or band areas (Table 1, Fig. 4).

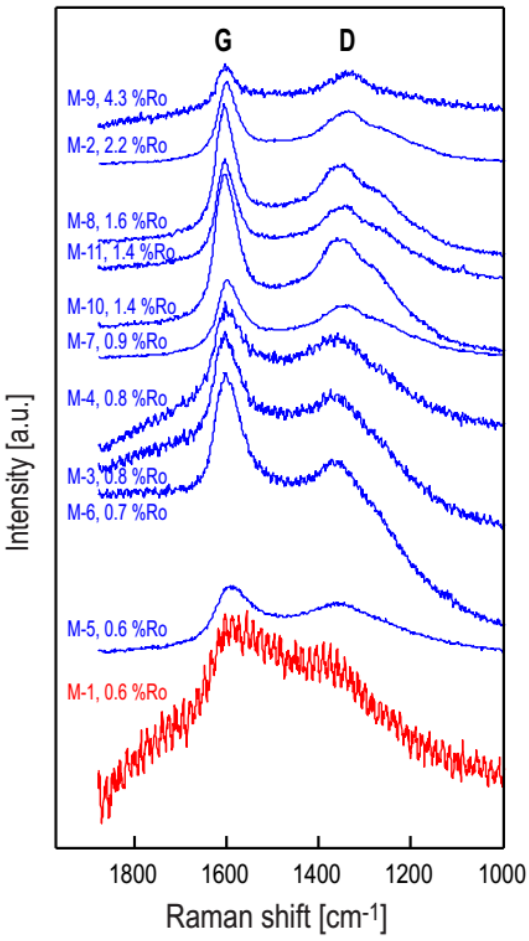

Fig. 2. Measured Raman spectra of organic-rich mudstones. The spectra are stacked in order of increasing thermal maturity (vitrinite reflectance) and offset for clarity. The spectra reveal the spread in the G and D band positions as a function of maturity.

The G and D1 band positions were, in general, readily determined from the Raman spectra without imposing any constraints on the curve fitting procedure (Fig. 3a). The resulting RBS increases systematically with increasing thermal maturity, with a tightly defined correlation (R^2 = 0.95; Fig. 3b). Sample M-1 (Type IIS kerogen) is excluded from this correlation because the extracted G band position could not be resolved with adequate accuracy and its RBS estimate falls off the trend. The root-mean-square-error (RMSE) of the RBS estimate from the correlation is 3.0 cm^{-1}. The uncertainty on the maturity estimate from RBS increases as maturity increases because of the logarithmic form of the regression. The estimated uncertainty (2σ) is ±0.25 % for samples with %VRe values of ~ 1 %, increasing to ±0.5 % or larger for samples with %VRe values above ~ 2 %. These uncertainties are on par with those for conventional vitrinite reflectance measurements (Hackey et al., 2015). The uncertainties on the Raman maturity estimates can likely be reduced by increasing the number of standards in the calibration, in particular for samples with thermal maturity > 2 %Ro.

It was found that the G and D1 band areas were more difficult to reliably determine than were their positions. The Raman spectra are a composite of multiple, overlapping bands (Fig. 1), and the fitted

peak areas are highly sensitive to signal-to-noise, the baseline correction, and the shape function (i.e., the shape of the curve allowed to fit each Raman band) (Lünsdorf et al., 2014). (The positions of the G and D1 bands and the RBS appear largely insensitive to these factors.) The unconstrained curve fitting procedure resulted in a large variability among the band areas from the 25 spectra acquired for each sample. Here, the D/G area ratio, $(D1/G)_{Area}$, was observed to increase with thermal maturity, albeit with significant error (Fig. 4a). This trend implies increasing disordering of the kerogen structure during maturation, which is inconsistent with recognized changes in kerogen structure including increasing aromaticity (Beyssac et al., 2002b; Lünsdorf et al., 2014). Other band ratios previously used for interpreting Raman spectra, such as R1 = $(D1/G)_{Intensity}$ and R2 = $(D1/[D1+D2+G])_{Area}$ (Beyssac et al., 2002b; Lünsdorf et al., 2014), were also examined for these samples without obtaining robust maturity correlations (Fig. 4b and 4c). The accurate determination of individual band areas and intensities appears challenging because of the broad and overlapping peaks in Raman spectra of kerogens, and thus the robustness of band ratios is questionable especially for less-ordered carbonaceous materials like kerogen (Wopenka and Pasteris, 1993). We note, for example, the very different position and peak shape of the poorly differentiated D2 band in the Raman spectra shown in Fig. 1. Different peak fits can be obtained by placing constraints (upper and lower bounds) on each of the peak parameters (position, FWHM, amplitude, shape function, etc.) in the fitting procedure, but caution is required in this instance because individual Raman peak parameters are not all known *a priori*.

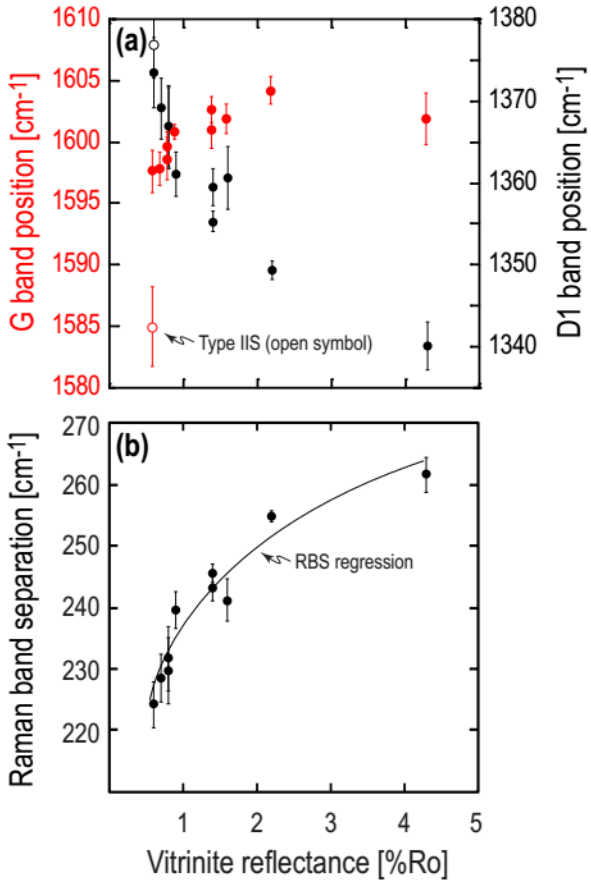

Fig. 3. Raman structural parameters plotted as a function of vitrinite reflectance: (a) G and D1 band positions, (b) Raman band separation (RBS). There is an excellent correlation between RBS calculated from the measured G and D1 band positions and vitrinite reflectance. The trend line is the best fit regression through the data.

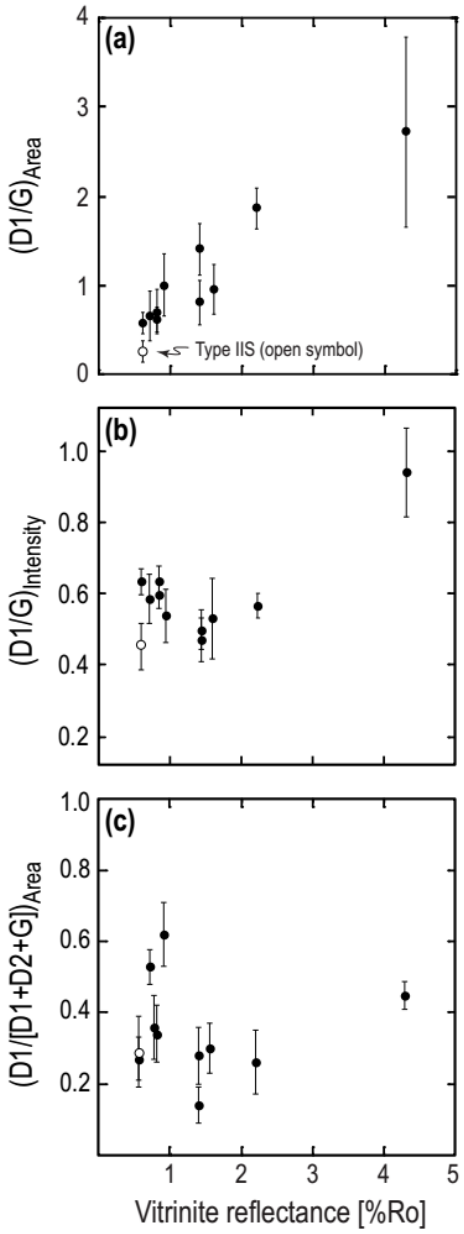

Fig. 4. Raman structural parameters plotted as a function of vitrinite reflectance: (a) D1/G area ratio, (b) D1/G intensity ratio, and (c) D1/(D1+D2+G) area ratio.

Fig. 5 overlays the correlation between RBS and thermal maturity for the organic-rich mudstones analysed in this study with RBS data reported by earlier studies (Kelemen and Fang, 2001; Schmidt Mumm and İnan, 2016; Spötl et al., 1998). The different datasets confirm the same, systematic trend. Our trend plots within the distribution of most other studies, but spans a wider range of maturities and shows a tighter correlation. The data of Schmidt Mumm and İnan (2016) show a parallel trend, but apparently offset toward higher RBS. Theirs are RBS estimates from the analysis of Silurian graptolites from the Qusaiba Formation in Saudi Arabia. This Silurian-age formation lacks vitrinite macerals, so vitrinite reflectance equivalent maturity estimates were derived from graptolite reflectance measurements for comparison with younger organic-rich mudstones. The different petrographic measurements used to determine vitrinite reflectance for the different

studies compared in Fig. 5 may factor into the offset trends. In addition, several studies have reported the wavelength dependence of the D band position in the Raman spectra of carbonaceous materials (the G band position is reported to be practically independent of the excitation energy) (Ferrari, 2002; Lünsdorf, 2016; Marshall et al., 2010; Matthews et al., 1999; Pócsik et al, 1998; Vidano, 1981; Wang et al., 1990). Schmidt Mumm and İnan (2016) used a laser wavelength of 632.8 nm, different to that used in our study (532 nm). However, Schmidt Mumm and İnan (2016) also reported the dispersion in their D band position as a function of laser wavelength between 488 and 788 nm (D band positions of 1338 and 1320 cm^{-1}, respectively), which allows their RBS values obtained at 632.8 nm to be recalculated to the laser wavelength of 532 nm used in our study. The dispersion in the D band amounts to 5.5 cm^{-1} between 632.8 and 532 nm, and when this adjustment is applied, the RBS values from Schmidt Mumm and İnan (2016) indeed move closer to the RBS data from our study (Fig. 6). On the other hand, the Raman measurements in this study and in that of Spötl et al. (1998) were obtained at nearly the same laser wavelengths (532 and 514.5 nm, respectively) and the two sets of RBS estimate overlay. The D band dispersion shown by earlier studies appear to fall along slightly different slopes (Fig. 7), indicating that the magnitude of the dispersion may be instrument specific and that no universal correction exists. The RBS data of Kelemen and Fang (2001) also overlay our RBS estimates, but these Raman data were acquired using a reported laser wavelength of 632.8 nm. Kelemen and Fang (2001) did not report D band dispersion as a function of laser wavelength, thus an instrument dispersion correction for better comparison is not possible for this data set. To a first order, it is seems possible to adjust RBS values obtained at different laser wavelengths to a common wavelength, although individual calibration of the magnitude of the D band dispersion as a function of laser excitation wavelength for kerogen of the similar maturity may be necessary for each Raman instrument.

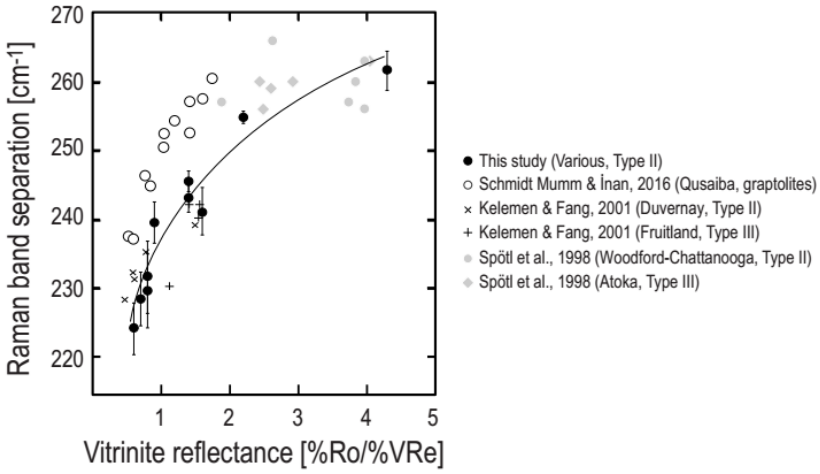

Fig. 5. Comparison of Raman band separation (RBS) for organic-rich mudstones from this and earlier studies. The data reveal the consistent trend of increasing RBS with increasing maturity.

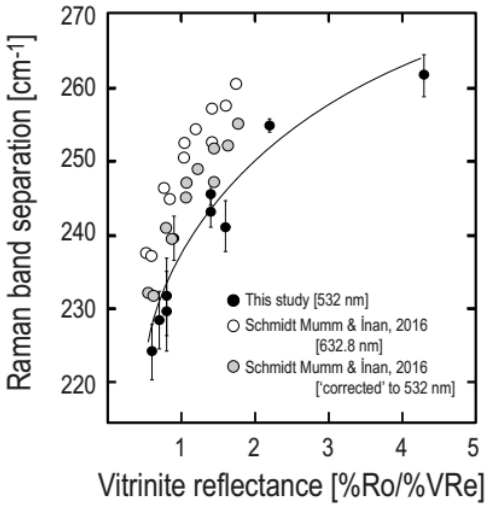

Fig. 6. Example of the laser wavelength dependent 'correction' to the Raman band separation.

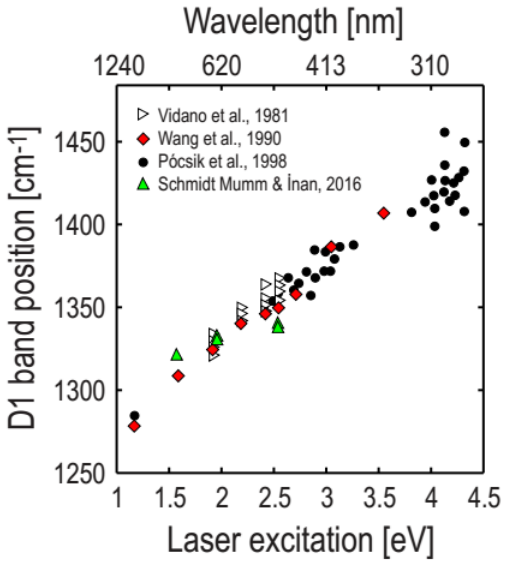

Fig. 7. Laser wavelength dependency of the D1 band position in carbonaceous materials from literature publications.

3.2. A rapid thermal maturity assessment using Raman spectroscopy

Several published Raman methods for thermal maturity estimations relied upon extensive sample preparation including embedding and polishing of bulk sample in resin (Lünsdorf, 2016; Schmidt Mumm and İnan, 2016), or isolation of kerogen from the bulk shale by concentrated HF/HCl treatment (Diessel et al., 1978; Spötl et al., 1998). By comparison, the Raman measurements in this study were made directly on drill core or cuttings chips without the need to cut and polish surfaces or to isolate kerogen. The shorter laser wavelength (532 nm) used here reduced background fluorescence (Lünsdorf, 2016) and, combined with automated fluorescence suppression, made it

possible to rapidly acquire reliable Raman spectra even for samples with low thermal maturity. The result is a robust correlation between RBS and thermal maturity spanning from at least 0.6 to 4.3 %Ro. The robust and quantitative relationship makes it possible to estimate vitrinite reflectance equivalent maturities and hydrocarbon type (i.e., oil, condensate, or gas window) from Raman measurements of unknown oilfield formation samples. Fig. 8 overlays the RBS maturity map with hydrocarbon typing based on thermal maturity windows for Type II kerogen presented by Tissot and Welte (1984). Moreover, the minimal and rapid sample preparation used here gives potential for the Raman maturity estimates to be made at the wellsite in near real-time, rather than in the laboratory weeks after the drilling process is complete.

The Raman method here has been applied to organic-rich mudstones with total organic carbon content of 4 wt% or above. This method with minimal sample preparation and no isolation of organic matter may be less practical for organic-lean samples (TOC < 2 wt%), due to lower signal-to-noise ratios of the respective Raman spectra. The method has been calibrated specifically on Type II kerogen that comprises mixed marine organic material (e.g., phytoplankton, zooplankton and bacteria) and is the most common type of sedimentary organic matter dispersed in petroleum source rocks. Only limited Raman data are available for the other principal kerogen types (i.e., lacustrine Type I and higher-order terrestrial Type III kerogen) that are less common in petroleum source rocks. Further study is necessary to establish RBS maturity maps for different organic matter types, since it is recognized that the windows for petroleum generation fall within different vitrinite reflectance values for the different kerogen types (Dembicki, 2009; Tissot and Welte, 1984).

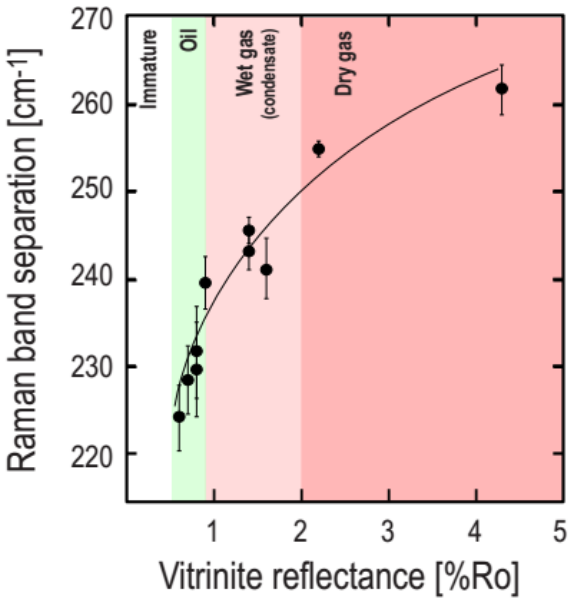

Fig. 8. Thermal maturity map for Type II kerogen. The Raman band separation can be used to determine the appropriate maturity window and hydrocarbon type in a petroleum source rock.

4. Conclusions

Raman spectroscopy is a powerful tool to assess the thermal maturity of kerogen in organic-rich mudstones. In particular, the Raman band separation (RBS, the shift between the G and D1 bands in Raman spectra) is a highly reliable estimate of thermal maturity. This study established a robust correlation (R^2 = 0.95) between RBS and thermal maturity expressed as vitrinite reflectance (%Ro) for a variety of paleo-marine petroleum source rocks spanning a wide range of maturity (0.6 to 4.3 %Ro). High-quality Raman spectra were acquired for the majority of samples by taking advantage of a short laser wavelength (532 nm) and successful Raman fluorescence suppression. The laser wavelength-dependence of the Raman D band position is one factor for observed differences in absolute RBS values as a function of thermal maturity among different laboratories. Accounting for this wavelength-dependence is necessary to develop universal correlation between RBS and thermal maturity expressed as vitrinite reflectance in organic-rich mudstones, independent of Raman instrumental protocols. Published Raman-based maturity estimations have largely relied on polishing of bulk rock fragments embedded in resin or the isolation of kerogen from the host rock by the use of concentrated acids. Our study shows that reliable Raman spectra can be acquired directly on drill core or cuttings of organic-rich formations without requiring such sample preparation. This opens the potential for rapid and non-destructive Raman measurements of petroleum source rocks directly at the wellsite for near real-time assessment of thermal maturity and hydrocarbon typing. The method here has been calibrated for Type II kerogen, which is the most relevant for the evaluation of petroleum source rocks. Further study is necessary to develop quantitative correlations between Raman signatures and thermal maturity in other types of sedimentary organic matter.

Acknowledgments

Brian Cardott (Oklahoma Geological Survey), Shell International Exploration and Production Inc., and the other oil companies are thanked for providing samples used in this project and for permission to publish. We highly appreciate the reviews received from anonymous reviewers, which greatly helped to improve this manuscript. We thank Prof. Ralf Littke for editorial handling.

References

Aloulou, F., 2015. Shale gas and tight oil are commercially produced in just four countries. U.S. Energy Information Administration, Independent Statistics and Analysis, February 13, http://www.eia.gov/todayinenergy/detail.php?id=19991 (accessed 20.11.16).

Behar, F., Beaumont, V., Penteado, H.L. De B., 2001. Rock-Eval 6 Technology: Performances and Developments. Oil & Gas Science and Technology - Revue de L'institut Francais du Petrole 56, 111-134, http://dx.doi.org/10.2516/ogst:2001013.

Beyssac, O., Rouzaud, J.N., Goffé, B., Brunet, F., Chopin, C., 2002a. Graphitization in a high-pressure, low-temperature methamorphic gradient: a Raman microspectroscopy and HRTEM study. Contributions to Mineralogy and Petrology 143, 19-31, http://dx.doi.org/10.1007/s00410-001-0324-7.

Beyssac, O., Goffé, B., Chopin, C., Rouzaud, J.N., 2002b. Raman spectra of carbonaceous material in metasediments: a new geothermometer. Journal of Metamorphic Geology 20, 859-871, http://dx.doi.org/10.1046/j.1525-1314.2002.00408.x.

Beyssac, O., Goffé, B., Petitet, J.-P., Froigneux, E., Moreau, M., Rouzaud, J.-N., 2003. On the characterization of disordered and heterogeneous carbonaceous materials by Raman spectroscopy. Spectrochimica Acta Part A: Molecular and Biomolecular Spectroscopy 59, 2267-2276, http://dx.doi.org/10.1016/S1386-1425(03)00070-2.

Blyth, F.G.H., de Freitas, M.H., 1984. A Geology for Engineers, 7th ed. Edward Arnold, London, ISBN 978-0713128826.

Bonijoly, M., Oberlin, M., Oberlin, A., 1982. A possible mechanism for natural graphite formation. International Journal of Coal Geology 1, 283-312, http://dx.doi.org/10.1016/0166-5162(82)90018-0.

Buseck, P.R., Huang, B.-J., 1985. Conversion of carbonaceous material to graphite during metamorphism. Geochimica et Cosmochimica Acta 49, 2003-2016, http://dx.doi.org/10.1016/0016-7037(85)90059-6.

Cardott, B.J., Kidwai, M.A., 1991. Graptolite reflectance as a potential thermal-maturation indicator, in: Johnson, K.S., (Ed.), Late Cambrian-Ordovician geology of the southern Midcontinent, 1989 Symposium. Oklahoma Geological Survey Circular 92, 203-209, ISSN 0078-4397.

Cesare, B., Maineri, C., 1999. Fluid-present anatexis of metapelites at El Joyazo (SE Spain): constraints from Raman spectroscopy of graphite. Contributions to Mineralogy and Petrology 135, 41-52, http://dx.doi.org/10.1007/s004100050496.

Cole, G.A., 1994. Graptolite-Chitinozoan Reflectance and Its Relationship to Other Geochemical Maturity Indicators in the Silurian Qusaiba Shale, Saudi Arabia. Energy Fuels 8, 1443-1459, http://dx.doi.org/10.1021/ef00048a035.

Dembicki, H., Jr., 2009. Three common source rock evaluation errors made by geologists during prospect or play appraisals. AAPG Bulletin 93, 341-356, http://dx.doi.org/10.1306/10230808076.

Diessel, C.F.K., Brothers, R.N., Black, P.M., 1978. Coalification and graphitization in high-pressure schists in New Caledonia. Contributions to Mineralogy and Petrology 68, 63-78, http://dx.doi.org/10.1007/BF00375447.

Ferralis, N., Matys, E.D., Knoll, A.H., Hallmann, C., Summons, R.E., 2016. Rapid, direct and non-destructive assessment of fossil organic matter via microRaman spectroscopy. Carbon 108, 440-449, http://dx.doi.org/10.1016/j.carbon.2016.07.039.

Ferrari, A.C., 2002. Determination of bonding in diamond-like carbon by Raman spectroscopy. Diamond and Related Materials 11, 1053-1061, http://dx.doi.org/10.1016/S0925-9635(01)00730-0.

Goodarzi, F., 1985a. Reflected light microscopy of chitinozoan fragments. Marine and Petroleum Geology 2, 72-78, http://dx.doi.org/10.1016/0264-8172(85)90050-9.

Goodarzi, F., 1985b. Dispersion of optical properties of graptolite epiderms with increased maturity in early Paleozoic organic sediments. Fuel 64, 1735-1740, http://dx.doi.org/10.1016/0016-2361(85)90401-6.

Grew, E.S., 1974. Carbonaceous Material in Some Metamorphic Rocks of New England and Other Areas. The Journal of Geology 82, 50-73, http://dx.doi.org/10.1086/627936.

Hackley, P.C., Araujo, C.V., Borrego, A.G., Bouzinos, A., Cardott, B.J., Cook, A.C., Eble, C., Flores, D., Gentzis, T., Gonçalves, P.A., Mendonça Filho, J.G., Hámor-Vidó, M., Jelonek, I., Kommeren, K., Knowles, W., Kus, J., Mastalerz, M., Menezes, T.R., Newman, J., Oikonomopoulos, I.K., Pawlewicz, M., Pickel, W., Potter, J., Ranasinghe, P., Read, H., Reyes, J., De La Rosa Rodriguez, G., Alves Fernandes de Souza, I. V., Suárez-Ruiz, I., Sýkorová, I., Valentine, B.J., 2015. Standardization of reflectance measurements in dispersed organic matter: Results of an exercise to improve interlaboratory agreement. Marine and Petroleum Geology 59, 22-34, http://dx.doi.org/10.1016/j.marpetgeo.2014.07.015.

Hood, A., Gutjahr, C.C.M., Heacock, R.L., 1975. Organic metamorphism and the generation of petroleum. AAPG Bulletin 59, 986-996, ISSN 1558-9153.

Hutton, A., Bharati, S., Robl, T., 1994. Chemical and Petrographic Classification of Kerogen/Macerals. Energy Fuels 8, 1478-1488, http://dx.doi.org/10.1021/ef00048a038.

Jarvie, D.M., Claxton, B., Henk, B., Breyer, J., 2001. Oil and Shale Gas from Barnett Shale, Ft. Worth Basin, Texas. AAPG National Convention, June 3-6, Denver, CO, USA, AAPG Search and Discovery Article #90906.

Kelemen, S.R., Fang, H.L., 2001. Maturity Trends in Raman Spectra from Kerogen and Coal. Energy Fuels 15, 653-658, http://dx.doi.org/10.1021/ef0002039.

Lafargue, E., Marquis, F., Pillot, D., 1998. Rock-Eval 6 Applications in Hydrocarbon Exploration, Production, and Soil Contamination Studies. Oil & Gas Science and Technology - Revue de L'institut Francais du Petrole 53, 421-437, http://dx.doi.org/10.2516/ogst:1998036.

Landis, C.A., 1971 Graphitization of dispersed carbonaceous material in metamorphic rocks. Contributions to Mineralogy and Petrology 30, 34-45, http://dx.doi.org/10.1007/BF00373366.

Liu, D., Xiao, X., Tian, H., Min, Y., Zhou, Q., Cheng, P., Shen, J., 2013. Sample maturation calculated using Raman spectroscopic parameters for solid organics: Methodology and geological applications. Chinese Science Bulletin 58, 1285-1298, http://dx.doi.org/10.1007/s11434-012-5535-y.

Liu, Y., Ferralis, N., Bryndzia, L.T., Grossman, J.C., 2016. Genome-inspired molecular identification in organic matter via Raman spectroscopy. Carbon 101, 361-367, http://dx.doi.org/10.1016/j.carbon.2016.02.017.

Lünsdorf, N.K., 2016. Raman spectroscopy of dispersed vitrinite – Methodical aspects and correlation with reflectance. International Journal of Coal Geology 153, 75-86, http://dx.doi.org/10.1016/j.coal.2015.11.010.

Lünsdorf, N.K., Dunkl, I., Schmidt, B.C., Rantitsch, G., von Eynatten, H., 2014. Towards a Higher Comparability of Geothermometric Data obtained by Raman Spectroscopy of Carbonaceous Material. Part I: Evaluation of Biasing Factors. Geostandards and Geoanalytical Research 38, 73-94, http://dx.doi.org/10.1111/j.1751-908X.2013.12011.x.

Marshall, A.O., Wehrbein, R.L., Lieberman, B.S., Marshall, C.P., 2012. Raman spectroscopic investigations of Burgess shale-type preservation: a new way forward. Palaios 27, 288-292, http://dx.doi.org/10.2110/palo.2011.p11-041r.

Marshall, C.P., Edwards, H.G.M., Jehlicka, J., 2010. Understanding the Application of Raman Spectroscopy to the Detection of Traces of Life. Astrobiology 10, 229–243, http://dx.doi.org/10.1089/ast.2009.0344.

Matthews, M.J., Pimenta, M.A., Dresselhaus, G., Dresselhaus, M.S., Endo, M., 1999. Origin of dispersive effects of the Raman D band in carbon material. Physical Review B 59, R6585-R6588, http://dx.doi.org/10.1103/PhysRevB.59.R6585.

McCarthy, K., Rojas, K., Niemann, M., Palmowski, D., Peters, K., Stankiewicz, A., 2011. Basic Petroleum Geochemistry for Source Rock Evaluation. Oilfield Review 23, 32-43, https://www.slb.com/resources/publications/industry_articles/oilfield_review/2011/or2011sum03_basic_petroleum.aspx (accessed 12.02.17).

Nishimura, Y., Coombs, D.S., Landis, C.A., Itaya, T., 2000. Continuous metamorphic gradient documented by graphitization and K-Ar age, southeast Otago, New Zealand. American Mineralogist 85, 1625-1636, http://dx.doi.org/10.2138/am-2000-11-1206.

Pasteris, J.D., Wopenka, B., 1991. Raman spectra of graphite as indicators of degree of metamorphism. Canadian Mineralogist 29, 1-9, ISSN 1499-1276.

Peters, K.E., 1986. Guidelines for evaluating petroleum source rock using programmed pyrolysis. AAPG Bulletin 70, 318-329, ISSN 1558-9153.

Peters, K.E., Walters, C.C., Moldowan, J.M., 2004. The Biomarker Guide: Volume 1, Biomarkers and Isotopes in the Environment and Human History, second ed. Cambridge University Press, Cambridge, England, ISBN 978-0521786973.

Petersen, H.I., Schovsbo, H.N., Nielsen, A.T., 2013. Reflectance measurements of zooclasts and solid bitumen in Lower Paleozoic shales, southern Scandinavia: Correlation to vitrinite reflectance. International Journal of Coal Geology 114, 1-18, http://dx.doi.org/10.1016/j.coal.2013.03.013.

Pócsik, I., Hundhausen, M., Koós, M., Ley, L., 1998. Origin of the D peak in the Raman spectrum of microcrystalline graphite. Journal of Non-Crystalline Solids 227-230, 1083-1086, http://dx.doi.org/10.1016/S0022-3093(98)00349-4.

Rantitsch, G., 1995. Coalification and graphitization of graptolites in the anchizone and lower epizone. International Journal of Coal Geology 27, 1-22, http://dx.doi.org/10.1016/0166-5162(94)00017-T.

Rantitsch, G., Grogger, W., Teichert, C., Ebner, F., Hofer, C., Maurer, E.-M., Schaffer, B., Toth, M., 2004. Conversion of carbonaceous material to graphite within the Greywacke Zone of the Eastern Alps. International Journal of Earth Sciences 93, 959-973, http://dx.doi.org/10.1007/s00531-004-0436-1.

Rantitsch, G., Lämmerer, W., Fisslthaler, E., Mitsche, S., Kaltenböck, H., 2016. On the discrimination of semi-graphite and graphite by Raman spectroscopy. International Journal of Coal Geology 159, 48-56, http://dx.doi.org/10.1016/j.coal.2016.04.001.

Schmidt Mumm, A., İnan, S., 2016. Microscale organic maturity determination of graptolites using Raman spectroscopy. International Journal of Coal Geology 162, 96-107, http://dx.doi.org/10.1016/j.coal.2016.05.002.

Spötl, C., Houseknecht, D.W., Jaques, R.C., 1998. Kerogen maturation and incipient graphitization of hydrocarbon source rocks in the Arkoma Basin, Oklahoma and Arkansas: a combined petrographic and Raman spectrometric study. Organic Geochemistry 28, 535-542, http://dx.doi.org/10.1016/S0146-6380(98)00021-7.

Tissot, B.P., Welte, D.H., 1984. Petroleum Formation and Occurrence: A New Approach to Oil and Gas Exploration. Springer-Verlag, Berlin, Heidelberg, New York, ISBN 3-540-13281-3.

Tuinstra, F., Koenig, J. L., 1970, Raman Spectrum of Graphite. The Journal of Chemical Physics 53, 1126-1130, http://dx.doi.org/10.1063/1.1674108.

Vidano, R.P., Fischbach, D.B., Willis, L.J., Loehr, T.M. 1981. Observation of Raman band shifting with excitation wavelength for carbons and graphites. Solid State Communications 39, 341-344, http://dx.doi.org/10.1016/0038-1098(81)90686-4.

Wang, Y., Alsmeyer, D.C., McCreery, R.L., 1990. Raman spectroscopy of carbon materials: structural basis of observed spectra. Chemistry of Materials 2, 557-563, http://dx.doi.org/10.1021/cm00011a018.

Wopenka, B., Pasteris, J.D., 1993. Structural characterization of kerogens to granulite-facies graphite: Applicability of Raman microprobe spectroscopy. American Mineralogist 78, 533-557, 0003-004X/93/0506-0533.

Yui, T.-F., Huang, E., Xu, J., 1996. Raman spectrum of carbonaceous material: a possible metamorphic grade indicator for low-grade metamorphic rocks. Journal of Metamorphic Geology 14, 115-124, http://dx.doi.org/10.1046/j.1525-1314.1996.05792.x.

Table 1. Geochemical characteristics of kerogen in organic-rich mudstones

Sample ID	Formation	OM Type	TOC [wt%]	Vitrinite reflectance[a]			Rock-Eval[b]			Raman					
				%*Ro* mean	*std*	*N*	*S2* [mg HC /g rock]	T_{max} [°C]	T_{max} maturity [% VRe]	G position, W_G [cm^{-1}]	D1 position, W_{D1} [cm^{-1}]	RBS, W_G-W_{D1} [cm^{-1}]	$(D1/G)_{Area}$	$(D1/G)_{Intensity}$	(D1/[D1-
M-1	Undisclosed	IIS**	15.7	0.55		-	129.5	416	0.3	1585.1 ± 3.2	1377.0 ± 4.1	208.0 ± 4.5	0.25 ± 0.12	0.45 ± 0.07	0.29
M-2	Marcellus	II	4.8	2.2		-	0.2	-	-	1604.3 ± 1.1	1349.5 ± 1.1	254.8 ± 0.9	1.87 ± 0.23	0.56 ± 0.03	0.26
M-3	Undisclosed	II	4.4	0.76	0.04	25	9.6	442	0.8	1599.7 ± 1.2	1367.0 ± 4.8	229.7 ± 5.4	0.70 ± 0.25	0.63 ± 0.04	0.36
M-4	Undisclosed	II	5.0	0.8	0.07	14	10.8	441	0.8	1598.7 ± 1.7	1367.0 ± 5.1	231.7 ± 5.3	0.61 ± 0.14	0.60 ± 0.04	0.34
M-5	Woodford	II	5.8	0.55		41	22.7	434	0.7	1597.7 ± 1.8	1373.5 ± 4.3	224.2 ± 3.7	0.57 ± 0.12	0.63 ± 0.04	0.27
M-6	Woodford	II	5.9	0.7		40	18.0	435	0.7	1597.9 ± 1.3	1369.3 ± 3.7	228.6 ± 3.9	0.66 ± 0.28	0.58 ± 0.07	0.53
M-7	Woodford	II	4.1	0.9		52	3.4	446	0.9	1600.9 ± 0.6	1361.3 ± 2.7	239.6 ± 2.9	1.00 ± 0.35	0.54 ± 0.07	0.62
M-8	Woodford	II	4.3	1.55		40	0.6	-	-	1601.9 ± 1.2	1360.7 ± 3.8	241.2 ± 3.5	0.95 ± 0.28	0.53 ± 0.11	0.30
M-9	Woodford	II	-	4.3	0.33	80	0.1	-	-	1601.9 ± 2.1	1340.2 ± 2.9	261.7 ± 2.8	2.72 ± 1.07	0.94 ± 0.13	0.45
M-10	Undisclosed	II	11.0	1.4	0.07	17	4.0	470	1.3	1602.7 ± 1.1	1359.6 ± 2.2	243.1 ± 2.0	0.81 ± 0.25	0.47 ± 0.06	0.14
M-11	Undisclosed	II	7.6	1.4		-	2.6	474	1.4	1601.0 ± 1.4	1355.4 ± 1.2	245.6 ± 1.4	1.41 ± 0.29	0.50 ± 0.06	0.28

[a]Vitrinite maceral count (*N*) and standard deviation (*std*) reported where provided as histograms by the laboratory

[b]Vitrinite reflectance equivalent from T_{max}: % VRe = [0.018*T_{max}]-7.16, from Jarvie et al. (2001)

**Type IIS kerogen omitted from the correlation

Graphical abstract

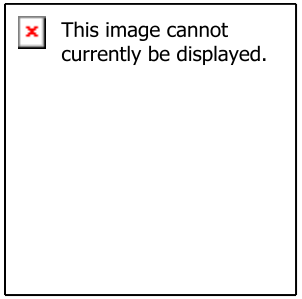

Manuscript Highlights

- Robust correlation of Raman signal and thermal maturity for organic-rich mudstones.
- Diverse sample set covering a broad range of maturities and geographical locations.
- Measured directly on cores and cuttings requiring only minimal sample preparation.